数理解析研究所講究録
993巻 1997年 26-34

Investigation of Shock-Wave Generation by a High-Speed Train Running into a Tunnel

Zonglin JIANG, Kei MATSUOKA, Akihiro SASOH and Kazuyoshi TAKAYAMA

Shock Wave Research Center, Institute of Fluid Science, Tohoku University
2-1-1 Katahira, Aoba-ku, Sendai 980-77, Japan

Abstract

This paper describes a numerical and experimental investigation into the shock-wave generation induced by a high-speed train running into a tunnel. Experiments were conducted by using a 1 : 300 scaled train-tunnel simulator. A dispersion-controlled scheme implemented with moving boundary conditions was used for solving the Euler equations assuming axisymmetric flows. Pressure histories at various stations with different distance from the entrance of a tunnel were obtained both numerically and experimentally for direct comparison. Good agreement between numerical and experimental results validated the observed nonlinear wave phenomena. More numerical calculations were carried out to interpret this wave propagation, and the compression-wave generation near the entrance of the tunnel was traced step by step to show development of the resulting weak shock wave. This study is meaningful not only for non-linear wave propagation in the train/tunnel dynamics but also for reduction of sonic booms in engineering applications.
Key Words: Train-tunnel dynamics, sonic booms, numerical simulations, a scaled train-tunnel simulator.

1. Introduction

Transportation systems need to be improved with quick development of modern societies. Among those systems, high-speed trains have been developed very rapidly in several countries in the world during the last three decades. The speed of these trains has been increased up to 270 km/h and are expected to reach 400 or 500 km/h in the near future. The trains moving at such a high speed may cause substantial aerodynamic problems like what once happened to airplanes. One of those problems is a "sonic boom" due to the shock wave driven by a train moving into a tunnel. Although the overpressure after the shock wave is relatively low, it is strong enough to produce loud noise and affect human eardrums. Therefore, this problem must be considered in designing such a new transportation system.

There was some pioneer research work relevant to this topic. Matsuo & Aoki[1] and Hage et al.[2] had numerically studied pressure wave propagation in tunnels, and flows in their study were modelled as one-dimensional compressible ones. Ogawa & Fujii simplified the problem as a two-dimensional inviscid flow[3], and the Euler equations were solved by a zonal method that can treat a moving grid configuration. Some experimental work was carried out by Sasoh et al.[4,5] using a train-tunnel simulator. The tunnel simulator was built up to a scale of 1 : 300 and shock waves were visualized with holographic interferometry. Because the flows in reality are very complex, the mechanism of the shock-wave generation still remains unclear.

In the present study, shock wave flows in tunnels were modelled as axisymmetric flows without considering viscous effects since viscosity is negligible in wave propagation in a short time duration. Because of the complicated shape of modern trains and the large ratio of the length to the diameter of a tunnel, it is almost impossible to do truly three-dimensional simulations even super-computers are available. Therefore, the axisymmetric assumption is a good approximation for time being. The computational domain of the simplified train-tunnel system is shown in Fig. 1. In order to simulate real cases and remove the blast waves created by suddenly starting of the train in numerical calculations, the train accelerated from a zero to given speed outside of tunnels, and then, moved into the tunnel at a constant speed.

The numerical code is designed based on the dispersion-controlled scheme[6,7] to avoid the numerical oscillations and need for additional artificial viscosity. In order to simulate a moving train, the surface of the train was traced

step by step while the train was moving in the fixed main mesh system. According to the position of the train, the moving boundary conditions consistent with the Euler equations were applied on surfaces of the train.

The experiments were conducted by using a scaled train/tunnel simulator. As it is known, viscosity can be neglected in propagation of shock waves driven by a piston and the relative wave phenomena are governed by the Euler equations which have no characteristic length. Therefore, the overpressure behind the shock waves simulated with this simulator can be expected to be similar to that in the real train-tunnel problem.

Two cases at train speed of 270 and 360 km/h, respectively, were simulated both numerically and experimentally. Pressure histories at various positions inside a tunnel were recorded. The obtained numerical and experimental results agree well with each other during the short period when and after the head of a train was entering the tunnel. A time sequence of pressure distributions of numerical results along the centerline of the tunnel were also produced to show the generation of compression waves and development of weak shock waves.

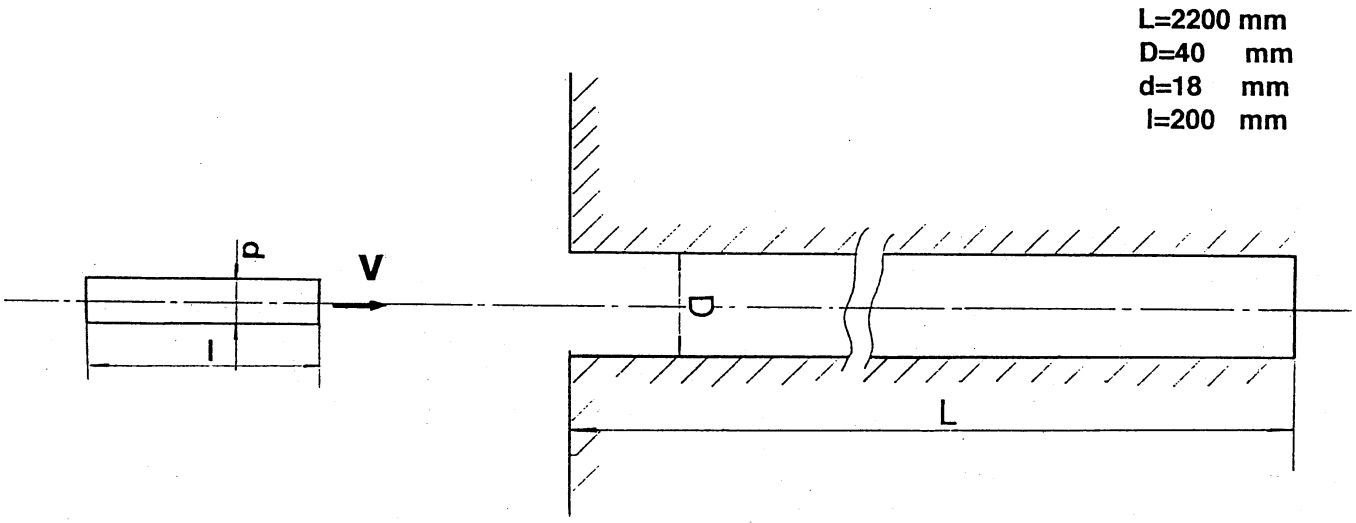

Fig. 1 Computational domain of the simplified train-tunnel system.

2. Numerical Methods

2.1 Governing equations

For axisymmetric flow problems, a hyperbolic system of conservation laws for perfect gas in cylindrical coordinates can be written as

$$\frac{\partial \mathbf{U}}{\partial t} + \frac{\partial \mathbf{F}}{\partial x} + \frac{\partial \mathbf{G}}{\partial r} + \frac{1}{r}\mathbf{S} = 0, \tag{1}$$

where $\mathbf{U}$, $\mathbf{F}$ and $\mathbf{S}$ denote the state variable, flux and source, respectively, given by

$$\mathbf{U} = \begin{pmatrix} \rho \\ \rho u \\ \rho v \\ e \end{pmatrix}, \quad \mathbf{F} = \begin{pmatrix} \rho u \\ \rho u^2 + p \\ \rho uv \\ (e+p)u \end{pmatrix}, \quad \mathbf{G} = \begin{pmatrix} \rho v \\ \rho uv \\ \rho v^2 + p \\ (e+p)v \end{pmatrix}, \quad \mathbf{S} = \begin{pmatrix} \rho v \\ \rho uv \\ \rho v^2 \\ (e+p)v \end{pmatrix}, \tag{2}$$

where primitive variables in the unknown $\mathbf{U}$ are density ρ, velocity components u and v, and total energy per unit volume e. p is fluid pressure and the equation of state for perfect gas is given as

$$e = \frac{p}{\gamma - 1} + \frac{1}{2}\rho(u^2 + v^2), \tag{3}$$

where γ, the specific heat ratio, is taken as 1.4 in the present calculations.

2.2 Dispersion controlled scheme

The explicit finite difference equations of Eqs.(1) discretized by using the dispersion controlled scheme are given in the form of half discretion as[6,7]

$$\left(\frac{\partial \mathbf{U}}{\partial t}\right)^n_{i,j} = -\frac{1}{\Delta x}(\mathbf{H}^n_{i+\frac{1}{2},j} - \mathbf{H}^n_{i-\frac{1}{2},j}) - \frac{1}{\Delta r}(\mathbf{P}^n_{i,j+\frac{1}{2}} - \mathbf{P}^n_{i,j-\frac{1}{2}}) - \mathbf{S}^n_{i,j}, \tag{4}$$

with

$$\mathbf{H}^n_{i+\frac{1}{2},j} = \mathbf{F}^+_{i+\frac{1}{2}L,j} + \mathbf{F}^-_{i+\frac{1}{2}R,j}, \qquad \mathbf{P}^n_{i,j+\frac{1}{2}} = \mathbf{G}^+_{i,j+\frac{1}{2}L} + \mathbf{G}^-_{i,j+\frac{1}{2}R}, \tag{5}$$

where

$$\begin{cases} \mathbf{F}^+_{i+\frac{1}{2}L,j} = \mathbf{F}^+_{i,j} + \frac{1}{2}\text{minmod}(\Delta\mathbf{F}^+_{i-\frac{1}{2},j}, \Delta\mathbf{F}^+_{i+\frac{1}{2},j}) \\ \mathbf{F}^-_{i+\frac{1}{2}R,j} = \mathbf{F}^-_{i+1,j} - \frac{1}{2}\text{minmod}(\Delta\mathbf{F}^-_{i+\frac{1}{2},j}, \Delta\mathbf{F}^-_{i+\frac{3}{2},j}) \end{cases}, \tag{6}$$

$$\begin{cases} \mathbf{G}^+_{i,j+\frac{1}{2}L} = \mathbf{G}^+_{i,j} + \frac{1}{2}\text{minmod}(\Delta\mathbf{G}^+_{i,j-\frac{1}{2}}, \Delta\mathbf{G}^+_{i,j+\frac{1}{2}}) \\ \mathbf{G}^-_{i,j+\frac{1}{2}R} = \mathbf{G}^-_{i,j+1} - \frac{1}{2}\text{minmod}(\Delta\mathbf{G}^-_{i,j+\frac{1}{2}}, \Delta\mathbf{G}^-_{i,j+\frac{3}{2}}) \end{cases}, \tag{7}$$

$$\begin{cases} \Delta\mathbf{F}^\pm_{i+\frac{1}{2},j} = \mathbf{F}^\pm_{i+1,j} - \mathbf{F}^\pm_{i,j} \\ \Delta\mathbf{G}^\pm_{i,j+\frac{1}{2}} = \mathbf{G}^\pm_{i,j+1} - \mathbf{G}^\pm_{i,j} \end{cases}, \tag{8}$$

$$\begin{cases} \mathbf{F}^\pm = \mathbf{A}^\pm\mathbf{U} \\ \mathbf{G}^\pm = \mathbf{B}^\pm\mathbf{U} \end{cases}. \tag{9}$$

The scheme is designed to meet dispersion conditions. Therefore, it is capable of capturing a discontinuity without numerical oscillations and additional artificial viscosity. The characteristic is very helpful to highlight development of the weak shock-wave. Steger and Warming's flux vector splitting was accepted in the computation[8]. Numerical solutions were marched in time using the second-order Runge-Kutta method. Reflecting boundary conditions were specified both on solid walls and the centerline of the computational domain. Non-reflecting boundary conditions were applied at the open area outside a tunnel, and the inflow and outflow boundaries. The calculations were carried out on an equally spaced grid with 200 × 7000 grid points.

2.3 Moving boundary conditions

In order to simulate a moving projectile, the surfaces of the projectile was traced step by step while the projectile was moving in the fixed main mesh system so that the moving boundary conditions consistent with the Euler equations can be applied on the surfaces of the projectile. The basic idea of the moving boundary conditions is shown in Fig. 2.

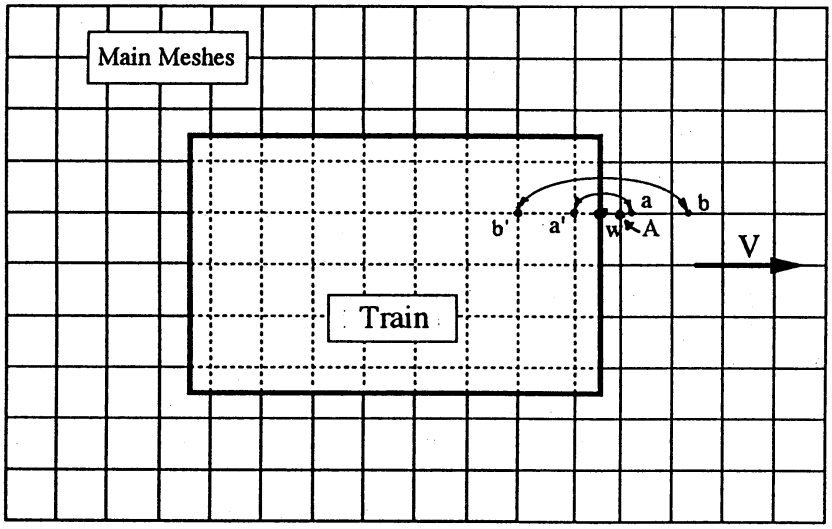

Fig. 2 Schematic diagram of moving boundary conditions

For example, to solve the governing equations at point A, flow states at point a' and b', which are within the boundaries of the projectile, are needed for our second-order scheme (it has a pencil of five points in each direction). Mirror images of these two points in the surface of the projectile are placed at a and b in the flowfield. This means that distances $aw = wa'$ and $bw = wb'$, and these lines are normal to the rigid wall. At each time step, positions

of point a and b were calculated first according to the moving surfaces, and then interpolation was applied to get flow states at these points. Finally, "mirror-image" flow states at virtual points were specified according to moving slip-boundary conditions, for example, at point a' as follows:

$$\begin{cases} u_{a'} = 2.0 * V - u_a, \\ v_{a'} = v_a, \\ \rho_{a'} = \rho_a, \\ p_{a'} = p_a, \end{cases} \tag{10}$$

where V is the speed of the projectile. This results in the surface of the projectile behaving like a moving solid wall. The number of the interpolated points needed depends on the order of accuracy of the numerical scheme.

3. Experiments

The experiments were conducted by using a 1 : 300 train/tunnel simulator in the Shock Wave Research Center, Tohoku University, Japan. This train/tunnel simulator consists of a driver section, an acceleration tube, a sabot separator, a test section and a piston recovery tank, as shown in Fig. 2. The piston is 18 mm in diameter and 40 mm in length. The test section is 40 mm in diameter and 25000 mm in length. This simulator was inclined at approximate 8° to the floor so as to make the gravitational force generated by the inclination compensate the loss of the piston speed due to friction from the direct contact between the steel test section and the plastic piston. Hence, experiments shown that the piston speed at the entrance was maintained almost constant after the piston went throughout the simulator. In experiments, pressure measurements along the test section were conducted for validation of numerical results and verification of appearance of shock waves in the tunnel.

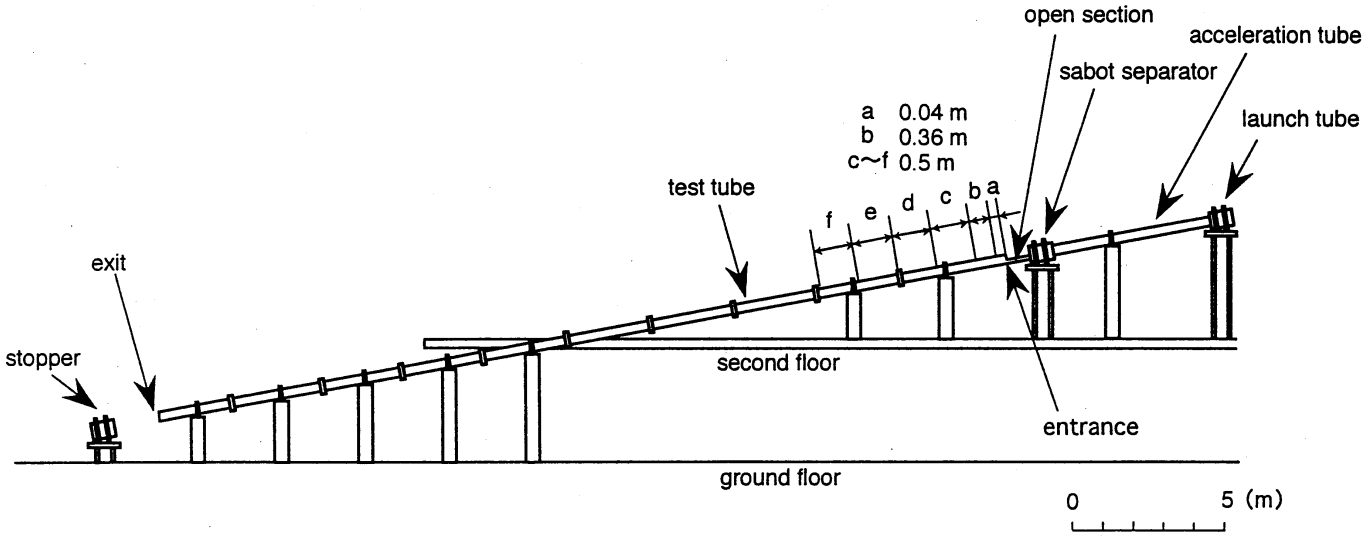

Fig. 3 Experimental set up of a scaled train-tunnel simulator

4. Results and Discussions

Some parameters in numerical calculations are as the followings: The diameter ratio of a train to a tunnel, d/D, is 0.45. The length of the train, l, is $5D$, and that of the tunnel, L, is $70D$. The reference length, d, is the train diameter. The train was accelerated from a zero to specified speed outside the tunnel to minimize the impulse pressure sign due to the suddenly starting of the train. The train speed maintains constant throughout the tunnel.

Figures 4 and 6 show numerical pressure histories inside a tunnel at various stations with different distances from the entrance. The relative experimental results were given in Figs. 5 and 7. The pressure histories in Figs. 4 and 5 were created with a train speed of 270 km/h and these in Figs. 6 and 7 did with a train speed of 360 km/h. Evidently, identical characteristics of the pressure histories can be found in these two pairs of figures. The numerical and experimental results agree well with each other. It was observed from these results that in the pressure history there is an impulse pressure sign followed by almost uniform pressure in front of the train. The impulse sign looks identical to each other for the relative numerical and experimental results both in Figs. 4 and 5 or Figs. 6 and 7.

The length of the uniform part behind the impulse sign varies depended on the position where pressure is measured, but it looks identical in the same measurement positions in numerical and experimental results.

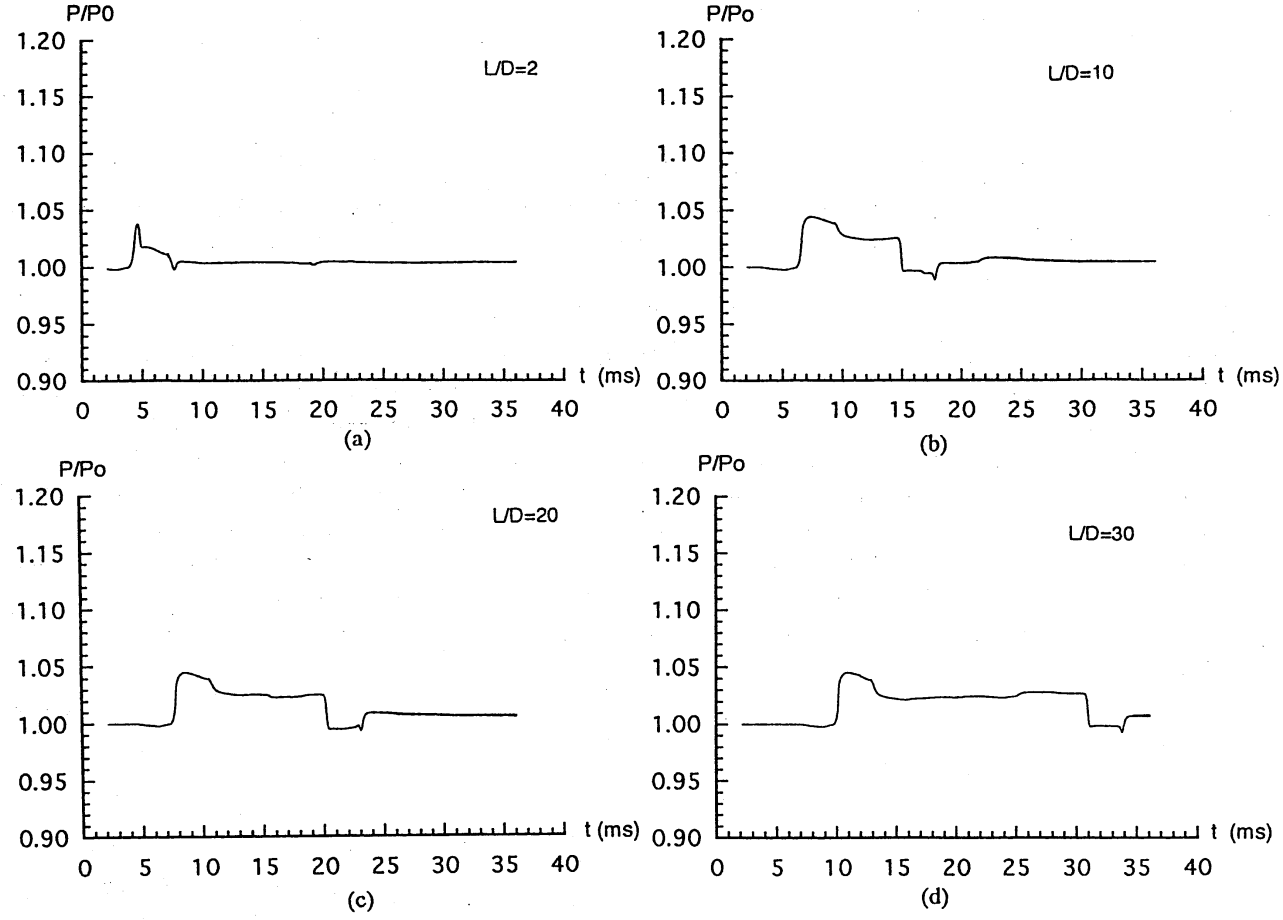

Fig. 4 Numerical pressure histories at various stations inside a tunnel, $V_t = 270\ km/h$

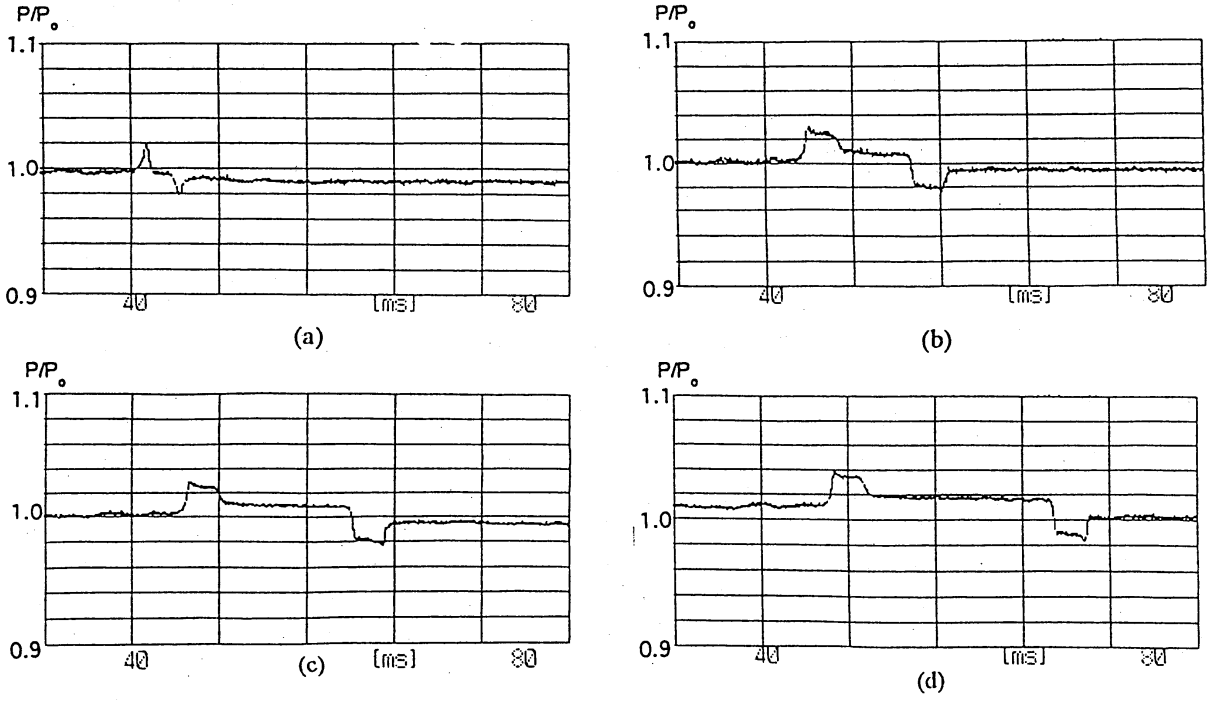

Fig. 5 Experimental pressure histories at various stations inside a tunnel, $V_t = 270\ km/h$

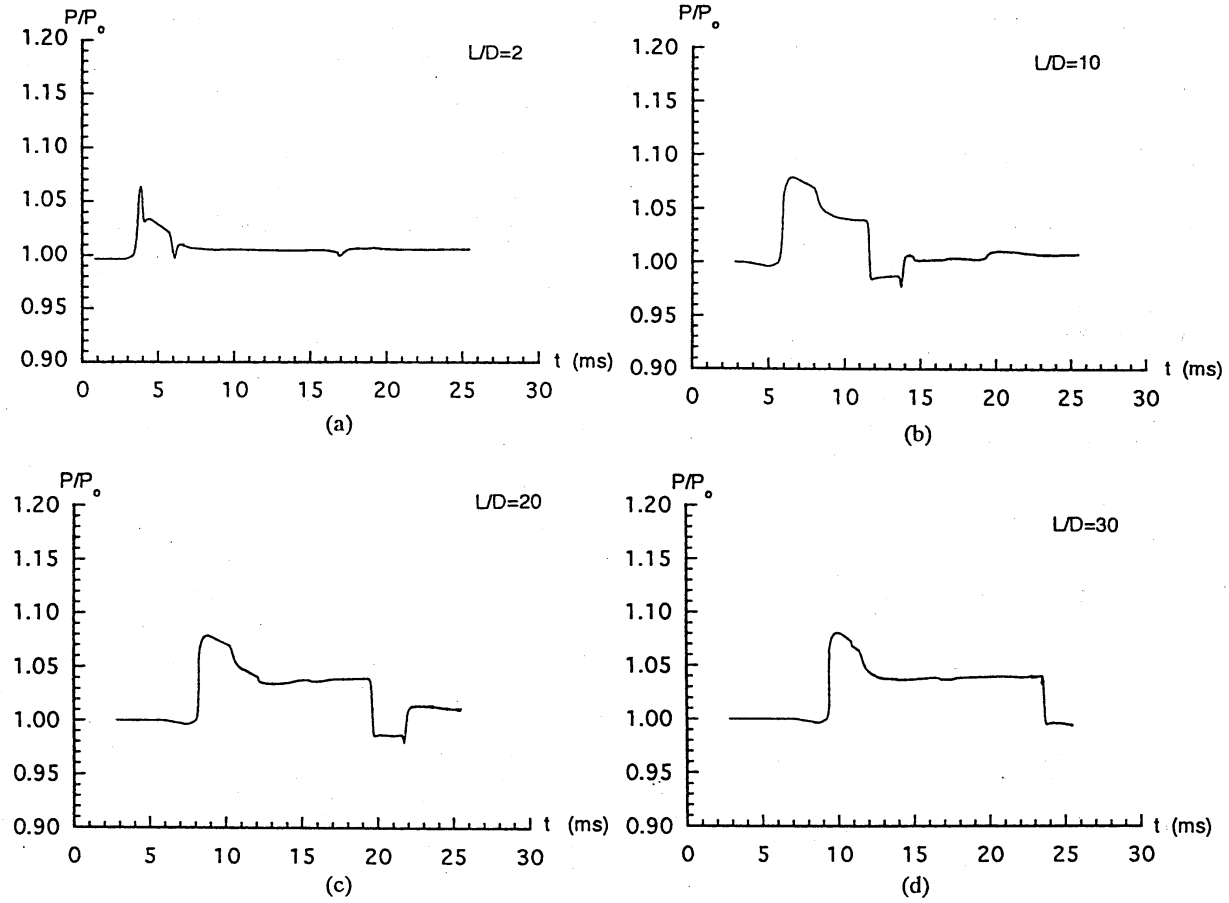

Fig. 6 Numerical pressure histories at various stations inside a tunnel, $V_t = 360\ km/h$

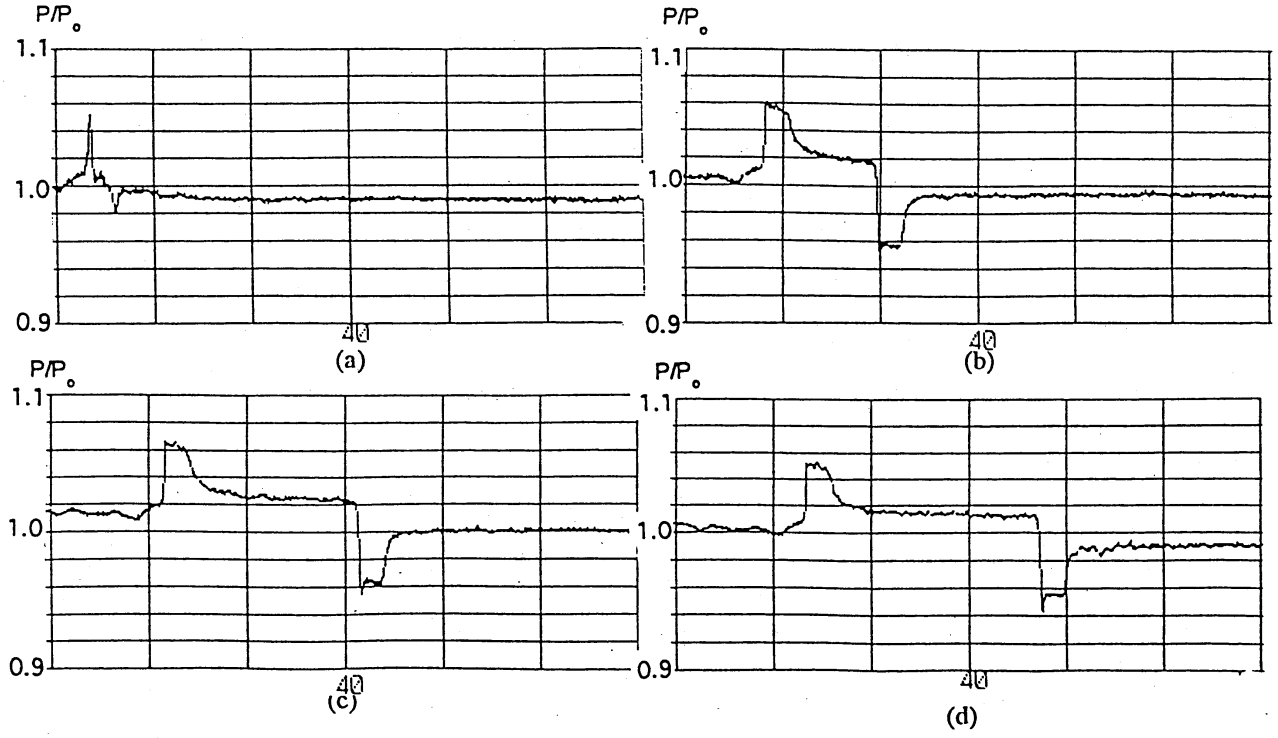

Fig. 7 Experimental pressure histories at various stations inside a tunnel, $V_t = 360\ km/h$

If carefully looking at the impulse pressure sign, it can be found that the sigh consists of three obvious parts. The first part is the peak pressure that is generated while the head of train is rushing into the entrance of a tunnel. The second one is gradually-decreased over-pressure that is created by transition from the suddenly-entering flow state to a stead-state resulting from an infinitely long train moving within a tunnel. The last one is quickly-decreased over-pressure due to the fact that expansion waves generated by entering of the tail of the train into a tunnel overtakes the train. The uniform part of the overpressure behind the impulse sign develops while the train moves inside of a tunnel. During this period, the flowfield around the train looks like a stead-state flow. The reason is that the constant drag force acting on the train provided energy and momentum for the uniform column of air ahead of the train. This phenomenon is consistent with conservation of momentum and energy.

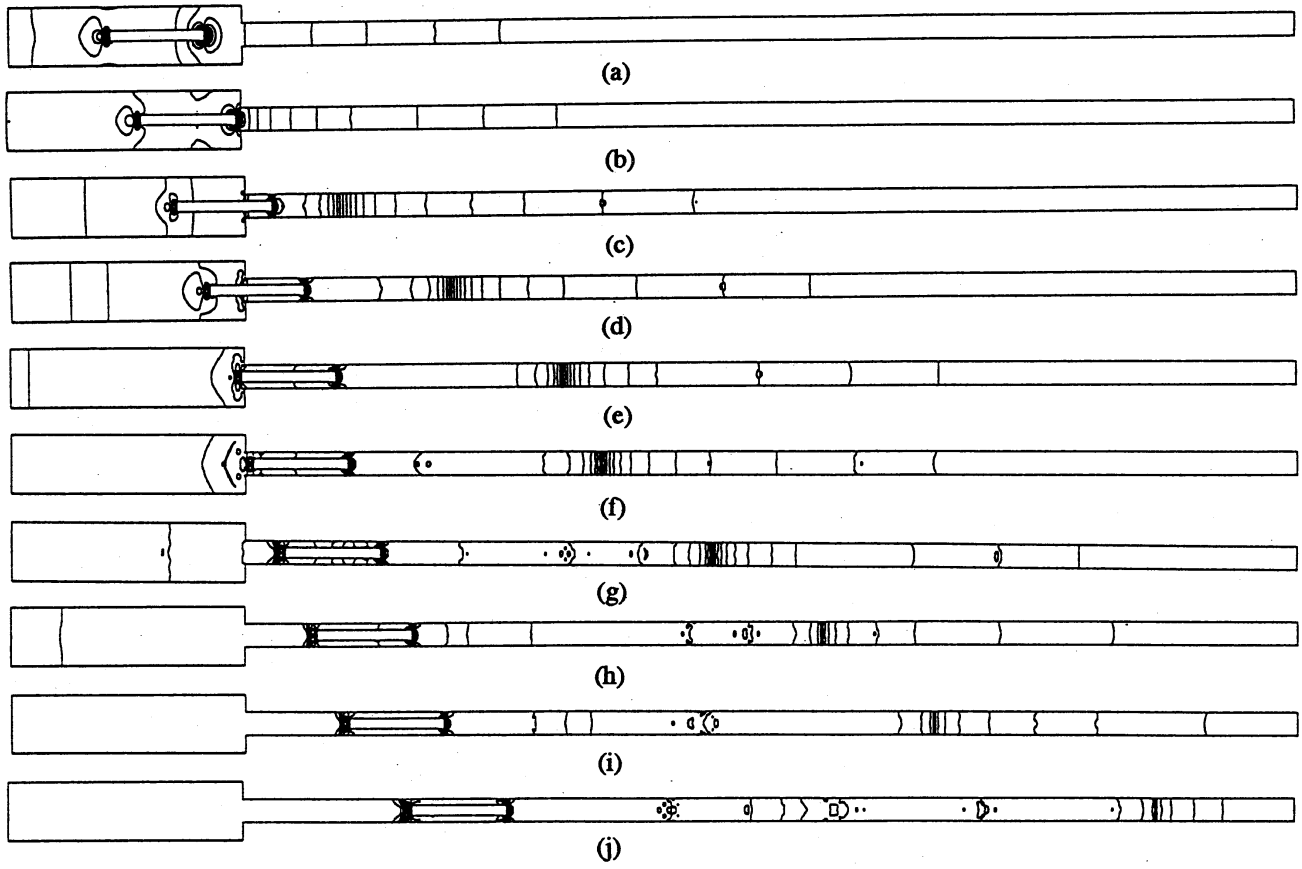

Fig. 8 Development of shock waves inside a tunnel, $V_t = 360\ km/h$

Figure 8 shows the build up of a series of compression waves ahead of a train while the train is rushing into a tunnel. The train speed in the case is 360 km/h and the train starts at the position from which the distance to the entrance of the tunnel is equal to the train length. Figure 9 shows a time sequence of pressure distributions along the axis of symmetry of a tunnel. There are ten frames in the figure and each of them is corresponding to that shown in Fig. 8 in time order.

Figure 8a shows the moment when the train was going to approach the entrance and the stagnation pressure in front of the train is shown in Fig. 9a. From the pressure distribution around the train and the stagnation pressure, the frame looks identical to a train moving in open space.

Figures 8b and 8c show the flowfield when the head of the train was entering the tunnel and a series of compression waves was produced in front of the train. The stagnation pressure also increases ai this moment as shown in Figs. 9b and 9c. This is due to the limited space in the tunnel entrance and reflection of compression waves.

From Figs. 8c to 8g, it can be seen that the isobars near the wave front got closer and closer because of non-linearity of compression waves. This phenomena can be also observed from the pressure distributions in Figs. 9c and 9g, where the compression wave front got steeper and steeper. Therefore, a shock wave developed gradually

due to this accumulation of the compression waves. The generated compression waves propagated at a sound speed so that the high pressure area became longer and longer. Flow transition from the suddenly-entering flow state to a stead-state resulting from an infinitely long train moving within a tunnel, as mentioned above, was also observed in Figs. 9e to 9g, where the overpressure behind the wave font decreased gradually.

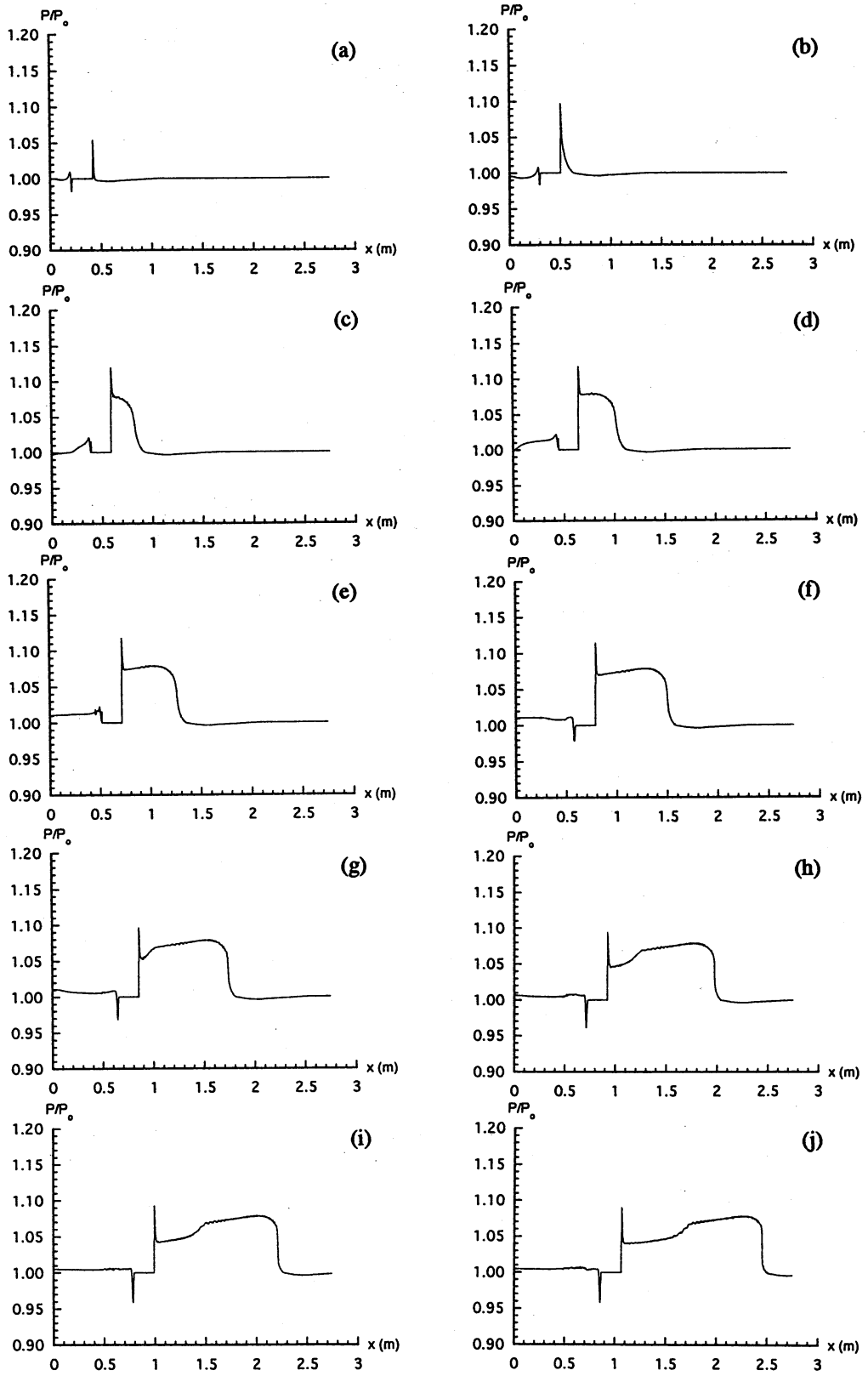

Fig. 9 A time sequence of pressure distributions along the axis of symmetry of a tunnel, $V_t = 360\ km/h$

Figure 8f shows that a series of expansion waves was generated behind the tail of the train due to suddenly entering of the rear of the train. These waves propagated forwards at sound speed and overtook the train later as shown in Figs. 8g to 8h. The effect of the expansion waves can be observed more clearly in Figs. 9g and 9f, where the overpressure ahead of the train reduced. This is the reason for creation of the third part of the impulse pressure sign observed both numerically and experimentally in Figs. 4 to 7.

An almost constant pressure behind the impulse pressure sign was observed in Figs. 8i and 8j and more clearly in Figs. 9i and 9j. This phenomonon is similar to a piston moving in a shock tube, in which a column of the air of uniform pressure was driven. The overpressure in the area is about 4.5% of the ambient pressure, and the overestimated pressure is less than 0.5% of the ambient pressure according to experiments[4]. Considering that this is an inviscid case, the results are in good agreement with the experiments.

From the discussions above, it is concluded that the impulse pressure sign is due to suddenly entering of the train into a tunnel. The resulting overpressure depends on the entrance configuration and the sign duration is related to the length of the train. As to the overpressure in the uniform part behind the impulse sign, it is mainly determined by the diameter ratio of the train to the tunnel. From the point of view, this understanding of the wave phenomenon shows us some measures for reducing the level of sonic booms. For instance, improvements on train shapes and entrance configurations of tunnels may efficiently reduce the impulse pressure sign, and perforated walls may be used to low the overpressure in the uniform part after the impulse pressure sign.

5. Conclusions

Flows driven by a high-speed train running into a tunnel are simulated successfully by dispersion-controlled scheme incorporated with moving boundary conditions. Numerical solutions are well validated by experiments. Both numerical and experimental results show that the overpressure in the train/tunnel problem consists of two parts. The first part is an impulse pressure sign due to suddenly entering of the head of a train. The other part of constant overpressure develops when the train is moving within a tunnel. The impulse sign is related to the shape of trains and tunnel configurations. The uniform pressure depends on the diameter ratio of the train and tunnel.

Reference

[1] Matsuo K. and Aoki T., Wave problems in high-speed railway tunnels, Proceedings of the 18th International Symp. on Shock Waves, Sendai, Japan, July 21–26, 1991, 95–102.

[2] Kage K., Miyake H. and Kawagoe S., Numerical study of compression waves produced by high-speed trains entering a tunnel, JSME international Journal, Series B, **2**(38), 191–198, 1955.

[3] Ogawa T. and Fujii K., Numerical simulation of compressible flows induced by a train moving into a tunnel, Computational Fluid Dynamics J., **1**(3), 63–82, 1994.

[4] Sasoh A., Onodera O., Takayama K., Kaneko R. and Matsui Y., Experimental study of shock wave generation by high speed train entry into a tunnel, Jpn Soc. Mech. Eng., **575**(60), 2307–2314, 1994.

[5] Sasoh A., Onodera O., Takayama K., Kaneko R. and Matsui Y., Experimental investigation on the reduction of railway tunnel sonic boom, Jpn Soc. Mech. Eng., **580**(60), 4112–4118, 1994.

[6] Zhang H.X. and Zhuang F.G., NND schemes and its applications to numerical simulation of two and three dimensional flows, Proceedings of 4th Inter. Symposium of CFD, Nagoya, Japan, 28–31, 1988.

[7] Jiang Z.L., Takayama K. and Chen Y.S., Dispersion conditions for non-oscillatory shock capturing schemes and its applications, Computational Fluid Dynamics J., **2**(4), 137–150, 1995.

[8] Steger J.L. and Warming R.F., Flux vector splitting of the inviscid gasdynamic equations with applications to finite difference methods, J. Comp. Phys., 40, 263–293, 1981.